

Characterization of Oxidation Kinetics and Oxide Scale Formation on Isothermal Oxidation of HR-120 Ni-based superalloy at 500°C

Noraziana Parimin^{a,*}, Esah Hamzah^b and Astuty Amrin^c

^aFaculty of Chemical Engineering & Technology, Universiti Malaysia Perlis (UniMAP), 02600 Arau, Perlis, Malaysia

^bFaculty of Mechanical Engineering, Universiti Teknologi Malaysia (UTM), 81310 Skudai, Johor, Malaysia

^cRazak Faculty of Technology and Informatics, UTM Kuala Lumpur, 54100 Kuala Lumpur, Malaysia

*Corresponding author. Tel.: +604-9798154; fax: +604-9798178; e-mail: noraziana@unimap.edu.my

ABSTRACT

The HR-120 Ni-based superalloy underwent isothermal oxidation at 500°C in order to better understand the oxidation kinetics and the production of oxide scales. To create small and large grain structure, the HR-120 Ni-based superalloy was heat-treated at two distinct temperatures, 950°C and 1100°C. A 500°C for 500 h isothermal oxidation test was performed on the heat-treated alloy of the study examined the oxidation kinetics, oxide phase development and oxide surface morphology of alloy that had undergone isothermal oxidation. Plotting weight gain versus surface area allowed for the measurement of oxidation kinetics. The XRD method was used to examine the oxide phase. Surface morphology was investigated with SEM and EDX methods. A parabolic rate law was observed in the oxidation of both heat-treated alloys, suggesting a diffusion-controlled oxide growth mechanism. The alloy's surface has developed many oxide phases as a result of exposures lasting 500 h. The oxidized samples' surface morphology after 300 hours shows that overly large Nb-rich oxides are dispersed throughout the continuous oxide scale development. On coarse-grained heat-treated alloys, Nb-rich oxides produced that were abnormally big. This occurrence will initiate a crack that spreads around the oxide.

Keywords: Ni-based superalloy, HR-120 alloy, Isothermal oxidation, Oxidation kinetic, Heat treatment

1. INTRODUCTION

HR-120 alloy is a Ni-based superalloy, used in high temperature application due to its excellent resistance to oxidation [1-3]. HR-120 alloy is a heat resistant alloy used for high temperature applications such as heating operations, furnace components and heat treatment operations [3]. High temperature oxidation resistance is one of the most important properties for high temperature applications. HR-120 alloy displays superior oxidation resistance to oxidizing environments. HR-120 alloy has the ability to form a protective oxide surface of oxide scale containing Cr at high temperatures which provides greater resistance to high temperature oxidation [3]. Protective Cr-containing oxide scale, Cr₂O₃, forms slowly and is excellently resistant to oxidation in a variety of hostile situations. In high-temperature applications, it is in charge of safeguarding metal alloys [4-7]. Many investigations related to chromium forming alloys report the formation of Cr₂O₃ and MnCr₂O₄, which act as a barrier against further oxidation and then offer high oxidation resistance [4,7-13]. The formation of oxides depends on the chemical composition, microstructure and the formation of alloy precipitates. Grain refinement was reported by other researchers as an approach to increase the oxidation resistance of alloys [14-16]. It's possible that fine grain size will significantly impact how the HR-120 alloy oxidizes. As a result, a heat treatment procedure was used on this project to alter the HR-120 alloy's grain size.

To form a stable precipitate during service, some alloying elements are usually added to the alloy such as, Nb, Ti and Mn [8,17-20]. Small amounts of Nb and Ti are often present in HR-120 alloy as alloying elements, which offer structural stability under harsh service circumstances [20]. The precipitation of carbides, such as MC carbides made of NbC, TiC, and/or (Nb,Ti)C, strengthens this alloy [19]. This HR-120 alloy experience very severe conditions at various temperatures and atmospheres during service. Due to oxidation at high temperatures, this alloy experiences a change in composition under these circumstances, resulting in the formation of an oxide layer. Therefore, it is important to know the behaviour of oxide scale formation in high temperature oxidation of HR-120 alloy.

2. MATERIALS AND METHODS

2.1. Material

The material used in this study is a HR-120 Ni-based superalloy with a chemical composition measured using an optical emission spectrometer (OES) presented in Table 1. The dimensions of the alloy are 10 mm x 10 mm x 3 mm.

Table 1 Chemical composition of HR-120 Ni-based superalloy

Element	Ni	Cr	C	Nb	Mn	Si	Ti	Al
Wt. %	40.4	24.1	0.05	0.44	0.70	0.44	0.03	0.08

*The balance is Fe

2.2. Methods

The HR-120 Ni-based superalloy is subjected to two distinct heat treatment processes in order to modify the alloy's grain size. The heat treatment process is carried out by heating the test sample at the treatment temperature for 3 hours of soaking time followed by rapid cooling in water. The grain size of the heat-treated samples was measured using the ASTM E112 linear intercept method. Small grains obtained from heat treatment at 950°C are designated as SG sample with an average grain size of 27.3 μm. Large grains labelled as LG sample was obtained on heat treatment at 1100°C with an average grain size of 36.3 μm.

Heat-treated SG and LG samples were subjected to isothermal oxidation tests at 500°C for 500 hours of exposure in laboratory air using a muffle furnace. The test sample underwent a grinding process until the surface finished of P600 grit. Each sample's surface area and weight were recorded before the isothermal oxidation test. The test samples were exposed to oxidation temperatures for a period of 100 hours to 500 hours following the discontinuous oxidation test method. The weight of the sample at each interval was recorded for determination of oxidation kinetics. An energy dispersive X-ray (EDX) spectrometer attached to a scanning electron microscope (SEM) was used to measure the oxide surface morphology. To conduct phase analysis, the X-ray diffraction (XRD) method was employed.

2.3. Equations

Equation (1) will be used to determine the oxidation rate law, where *t* is the time, *c* and *m* are constants, and *x* is the weight change per surface area. The value of *m* determines the oxidation rate law; a value of 1 denotes a linear rate law, and a value of 2 denotes a parabolic rate law. During the analysis, we used a range of *m* values to determine the rate law, that is, the *m* value for the linear rate law was from 0.50 to 1.49 and the *m* value for the parabolic rate law was from 1.50 to 2.49. Equation (2) is used to determine the parabolic rate constant, *K_p* value.

$$\log x = \left(\frac{1}{m}\right) \log t + c \tag{1}$$

$$x^2 = K_p t + c \tag{2}$$

3. RESULTS AND DISCUSSION

The oxidation kinetics of SG and LG samples oxidized at 500°C are shown in Figure 1. The pattern of weight change for both samples show an increasing trend as the exposure

period increases. Small grain SG samples recorded lower weight gain values than large grain LG samples. The low weight pattern of the SG sample is occupied by the fast outward diffusion of metal ions to the metal-atmosphere interface through short-circuiting action. Grain boundaries act as short circuit diffusion paths. The alloy's small grain size dominates the diffusion along this pathway. Grain boundary areas are more in alloys with smaller grains. With the fast diffusion of ions, the formation of the initial oxide layer is faster, then it will protect the component from further oxidation process. This initial oxide layer formed in less than 100 minutes as observed in our previous research using thermogravimetric analysis (TGA) [21]. Therefore, the oxidation kinetics of the SG sample did not show an increase in the weight gain at the initial stage of 100 hours of exposure compared to the LG sample. As the protective oxide scale grows faster, the following oxide growth will slow down, as it reaches the optimum oxide thickness to coat the alloy surface. Therefore, small grains recorded a lower weight gain. This phenomenon has been found in our previous works on other Ni-based alloys consisting of Fe-Ni-Cr, where the fine grain alloy structure will dominate the thin oxide scale, thus recording a low weight change on the oxidation kinetic curve [7].

On the other hand, large alloy grain size LG sample shows a high weight gain pattern. This is due to the continuous growth of oxides to develop oxide scale, to produce a protective layer on the surface of the alloy. The higher oxidation kinetics indicates that the LG sample has a thick oxide scale formed on the surface of the alloy. In contrast to the small grain size, this large grain size alloy has less grain boundary area, hence less short circuit diffusion paths in the alloy structure. Therefore, the formation of oxide scale will continue, thus recording a high weight gain.

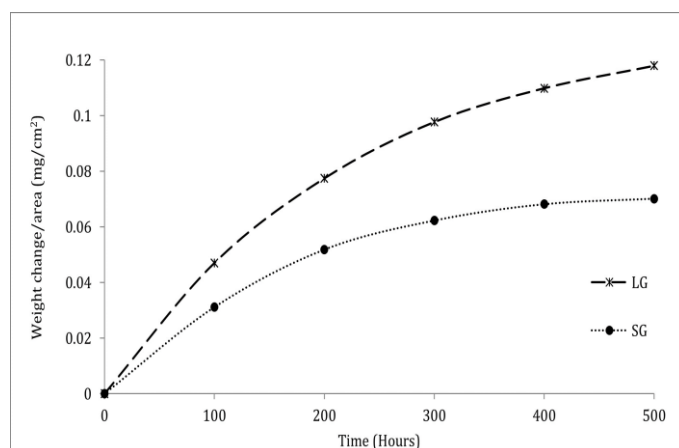


Figure 1. Oxidation kinetics.

The oxidation rate can be determined by using the identification of the oxidation rate law. The determination of the oxidation rate law is according to equation (1), as shown in Figure 2. The double log plot in Figure 2 shows that both samples follow a parabolic rate law, with *m* values equal to 1.95 and 1.73 for SG and LG samples, respectively. The values of *m* for these two samples are in the range of 1.50 to 2.49, which lies under the parabolic rate law. In addition, both samples also have good fitting parameters

which are R^2 values of 0.95 and 0.98, indicating that the data obtained in both samples have a high consistency with the curve plotted in the graph.

The parabolic rate constants for SG and LG samples were determined by square graph analysis in Figure 3, according to the method of equation (2). Both samples show good matching results for R^2 values. The small grain SG sample showed a low parabolic rate constant value of $2.739 \times 10^{-9} \text{ mg}^2\text{cm}^{-4}\text{s}^{-1}$. A low value of the parabolic rate constant indicates that a low rate of oxidation occurs in this sample. This phenomenon shows good oxidation resistance, therefore has good alloy protection. On the other hand, the large grain LG sample recorded a higher parabolic rate constant value of $8.184 \times 10^{-9} \text{ mg}^2\text{cm}^{-4}\text{s}^{-1}$, indicating a high oxide growth rate dominated by this sample. This analysis is consistent with the results of oxidation kinetics recorded in both samples.

A low rate of oxidation has occurred when the parabolic rate constant is low. A mechanism of oxide growth rate that is known to be diffusion-controlled is the parabolic rate law. That is, as the exposure period continues, the oxide scale formation will slow down as it reaches the optimum thickness. When optimal protection has been achieved, the rate of oxidation will slow. The lower the value of the constant, the lower the rate of oxidation occurs, which is the desired result in this work to achieve good oxidation resistance. This phenomenon was recorded in small grain SG samples in this work.

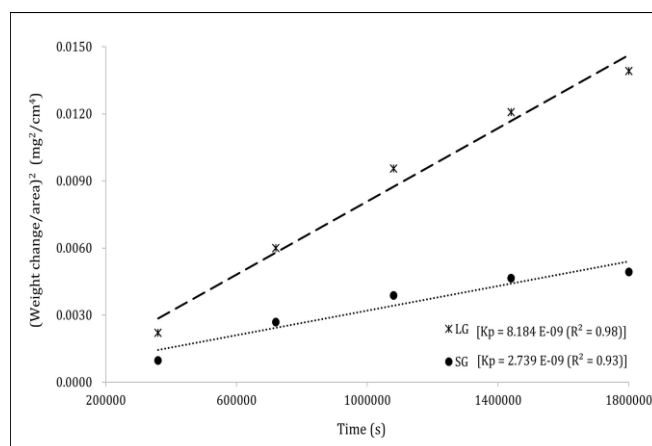


Figure 3. Parabolic rate constant.

Phase analysis was determined using the XRD technique for SG and LG samples after 500 hours of exposure. The XRD analysis is shown in Figure 4. The analysis records the formation of the main Cr-containing oxides Cr_2O_3 and MnCr_2O_4 oxides. These oxide phases are known for their protective behavior [4,7-13]. The development of Cr-Mn oxide indicates that the oxide scale that formed on the sample's surface has good protective characteristics. Several studies [9,12] claim that Mn increases the formation of Cr-Mn spinel oxide in the Fe-Ni-Cr alloy system, which can lessen the impact of Cr volatilization at high temperatures. In addition, there is the detection of other phases forming the base metal, indicating that a thin oxide scale has formed on the surface of the alloy.

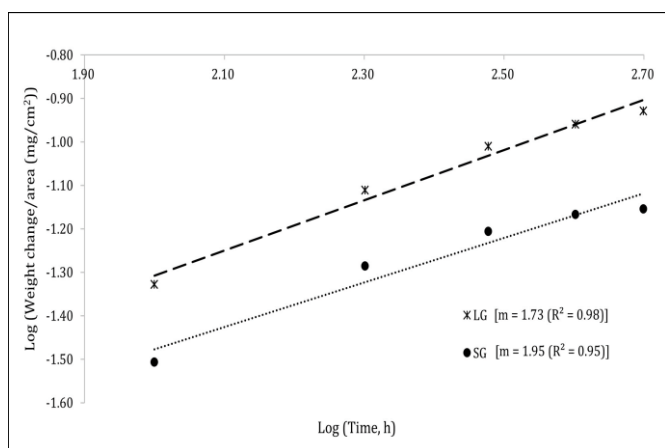


Figure 2. Oxidation rate law.

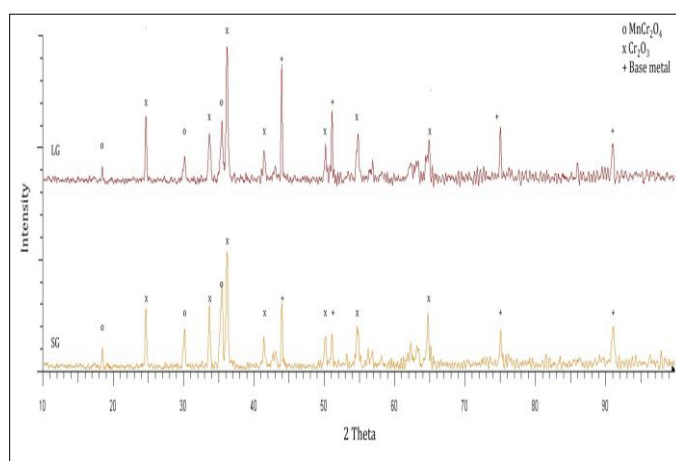


Figure 4. XRD analysis.

Oxide morphology analysis using a scanning electron microscope (SEM) equipped with an energy dispersive x-ray (EDX) spectrometer was performed on oxidized samples at 300 hours and 500 hours exposure as shown in Figures 5 and 6. Figures 5(a) and (d) show the development of continuous oxide scales on the alloy's surface on the SG and LG samples. The images also show the formation of oxide precipitates that grow prominent on the surface. A close-up image with higher magnification is shown in Figure 5 (b). The structure of the prominent white precipitate was further analyzed using the EDX technique (Figure 5 (c)), resulting in the determination of the main elements Nb and

O in region A. This observation suggested the formation of Nb-rich oxides. In addition, EDX analysis revealed trace amounts of Ni, Cr, Ni, and Mn, indicating the formation of Cr and Cr-Mn oxides in conjunction with the identification of the primary base metal content as determined by XRD analysis.

The XRD method cannot detect the limited amount of Nb-rich oxide precipitates on the alloy surface due to their micron and sub-micron size. This Nb-rich oxide can be analysed by EDX technique. Other researchers also found that Nb-rich oxide precipitated on the oxidized surface of the alloy 718 composed of Ni-19Cr-18Fe-5Nb-3Mo, but could not be detected using XRD, so it was further analysed using EDX analysis [20].

Figure 6 illustrates the analysis of oxide scale formation after 500 hours of exposure. It displays the formation of a uniform oxide layer coexisting with excessively large oxide particles rich in Nb that have a protruding structure. A key observation is that the size of Nb-rich oxides is larger on the large grain LG sample than on the small grain SG sample. This observation suggests that the oxide scale's ideal growth was dominated in the small grain SG sample as observed by the oxidation kinetics of this sample, showing a lower weight gain, therefore having a thin oxide scale. Whereas, in addition to the excessively large precipitate structure on the large grain LG sample, there is also the formation of cracks around the excessively large precipitate with protruding structure as noted in the red line of the rounded rectangle in Figure 6 (b).

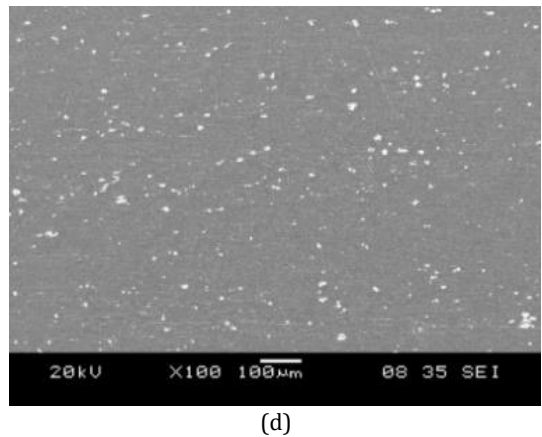
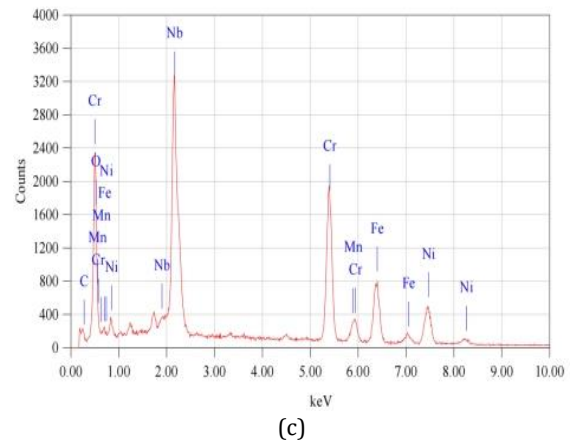
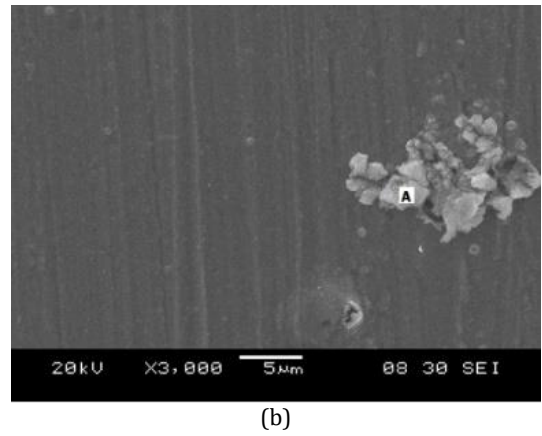
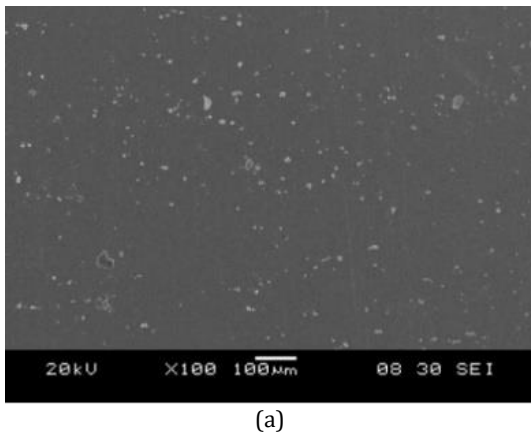
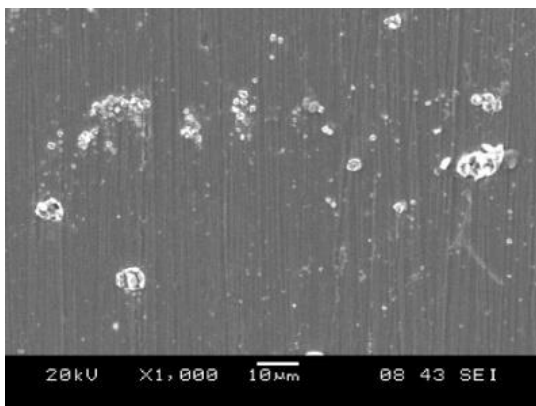
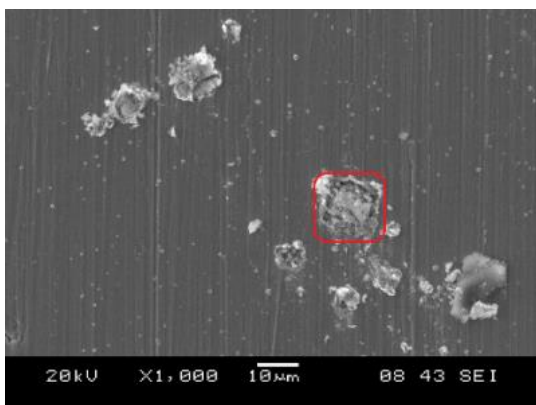


Figure 5. Oxidized sample after 300 hours; (a-c) SEM-EDX images of SG and (d) SEM image of LG.



(a)



(b)

Figure 6. Oxidized sample after 500 hours; (a) SEM image of SG and (b) SEM image of LG.

The formation of excessive Nb-rich oxide with a protruding structure is illustrated in the physical diffusion model for the formation of Nb-rich oxide as shown in Figure 7. Figure 7 (a) to (f) represents the exposure of HR-120 Ni-based superalloy at high temperature, recommend at 500°C with extended exposure time. The exposure period is not subject to a specific time. When the alloy is subjected to high temperature conditions at the start of the oxidation process in Figure 7(a), oxide nuclei start to form. The formation of oxide nuclei is produced by the outward diffusion of metal ions (M^+) from the base metal to the metal-atmosphere interface, where there is a supply of oxygen, O_2 in the atmosphere. Oxide nucleation is dominated by outward diffusion through the alloy matrix and short circuit diffusion, such as grain boundary regions. Additionally, the existence of MC precipitates in this alloy such as NbC and/or (Nb,Ti)C is also illustrated, and labeled in the figure. MC precipitates containing Nb tend to supply Nb ions towards the alloy surface, combining with oxygen ions from the atmosphere to form Nb-rich oxides as illustrated in Figure 7 (b).

As the oxidation process is prolonged, lateral oxide growth takes its place in the growth mechanism, increasing the amount of continuous oxide layer that is established on the surface by the fusion mechanism, as illustrated in Figure 7 (c). Adjacent oxide nuclei will grow laterally and collide with each other to form a continuous oxide structure. This action will form a protective oxide layer that will cover the entire surface of the alloy. The oxide scale developed is a

mixed structure of Cr-containing oxides and Nb-containing oxide phases. Vertical oxide growth will occur after lateral oxide growth in order to further expand the oxide scale and improve the optimum oxide thickness in order to obtain optimum protection. Vertical oxide growth is illustrated in Figure 7 (d). The vertical growth mechanism will continue to occur at oxidation temperatures and during extended oxidation periods.

Literally, vertical oxide growth can be divided into two types, which are subject to fine grain structure and coarse grain structure. Fine grain structures have high grain boundary areas that act as short circuit pathway for metal ion diffusion. The higher area will dominate the rapid initial oxide formation on the alloy surface, thereby accelerating the continuous oxide layer. As a continuous oxide layer forms, it encases the alloy and acts as a protective barrier between the base metal and the environment. When the protective barrier is reached, the formation of oxide scale to increase the thickness will also hold back, therefore dropping the oxidation rate. This phenomenon is shown by the low parabolic rate constant for the small grain SG sample, and also the lower weight gain on the oxidation kinetic curve. A parabolic rate constant with lower weight gain was desired in this study because this sample has optimum oxidation resistance. On the other hand, coarser grain sizes will behave differently, displaying a higher weight gain on the oxidation kinetic curve and a higher parabolic rate constant, indicating a high oxidation rate. A high oxidation rate will dominate the formation of oxide scale for it to occur continuously, thus thickening the oxide layer.

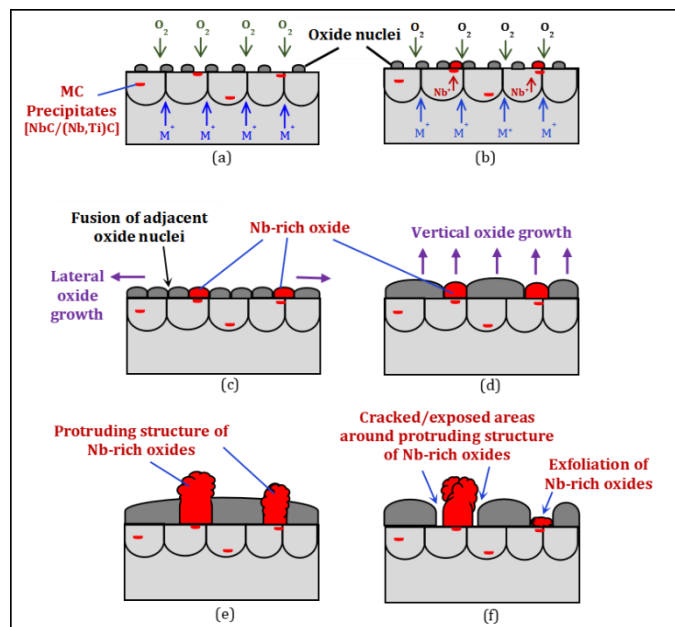


Figure 7. A physical diffusion model for the formation of Nb-rich oxides.

Figure 7 (e) shows the formation of Nb-rich oxide with a protruding structure as the oxidation period increases. These protruding structures stick together with other oxide phases forming a continuous oxide scale. This phenomenon can be seen in the SEM images of the SG and LG samples in

Figure 5 at an exposure period of 300 hours. When the exposure time is extended as shown in Figure 7 (f), the Nb-rich oxide particles continue to grow to form overgrown oxide particles. The oxide growth rate of Nb-rich oxides is higher than that of other Cr-containing oxide phases. This effect will cause the formation of cracks around the overgrown structure due to different growth rates as shown in the red line of the rounded rectangle in Figure 6 (b). As the Nb-rich oxide continues to grow, the larger oxide particles tend to lose contact with the base metal, with the addition of cracks around the particles that stop bonding between the oxide phases. This will cause the formation of oxide exfoliation. In addition, the establishment of cracks around the overgrown oxide particle also causes the protective behavior to decrease due to the exposed area on the cracked regions. When the unprotected area is exposed, new oxide nuclei will form to cover the exposed area. This phenomenon will cause an increase in the oxide scale formation, therefore increasing the weight change of the oxide, as recorded on the oxidation kinetics of the LG sample in Figure 1.

As a result, the formation of Nb-rich oxide particles on the coarse grain structure will lead to the formation of unstable oxide growth, which in a certain period of time will reduce the protective behavior of the oxide scale caused by oxide exfoliation. This result is in line with the findings in the SEM image in Figure 6 (b). In addition, the development of overgrown Nb-oxide structures has also been testified in our previous finding, which indicates the formation of cracks and exfoliation of the Nb-rich oxide structure dominated by the coarse grain structure [3,13].

4. CONCLUSION

The isothermal oxidation test has been successfully studied in this work. Small grain SG samples exhibited good oxidation resistance with low weight change and low parabolic rate constant values. In addition, a uniform oxide scale consisting Cr-containing oxides with coexisting Nb-rich oxide precipitates was formed on the surface of the alloy. On the other hand, the large grain LG sample showed a higher oxidation rate with a high weight change and a high parabolic rate constant value. In addition, this large grain LG sample records cracks around overgrown Nb-rich oxides with protruding structures.

ACKNOWLEDGMENTS

The authors would like to acknowledge the Ministry of Higher Education Malaysia for supporting their research by providing funding from the Fundamental Research Grant Scheme (FRGS), grant number FRGS/1/2020/TK0/UNIMAP/02/43.

REFERENCES

- [1] C. N. Athreya, K. Deepak, D. I Kim, , B. Boer, S. Mandal, and V. S. Sarm, "Role of grain boundary engineered microstructure on high temperature stream oxidation behavior of Ni based superalloy alloy 617," *Journal of Alloys and Compounds*, vol. 778, pp. 224-233, 2019.
- [2] K. E. Tillous, J. Dulcy, and T. Belmonte, "Degradation Behaviour of HR-120 Alloy Exposed to CH₄-CO-H₂-H₂O Mixed-Gas Environments at 950 °C," *Oxidation of Metals*, vol. 82, pp. 163-179, 2014.
- [3] N. Parimin, and E. Hamzah, "High Temperature Isothermal Oxidation of Heat-treated HR-120 Ni-based Alloys," *IOP Conference Series: Materials Science and Engineering*, vol. 864, no. 012116, 2020.
- [4] A. Col, V. Parry, and C. Pascal, "Oxidation of a Fe-18Cr-8Ni austenitic stainless steel at 850 °C in O₂: Microstructure evolution during breakaway oxidation," *Corrosion Science*, vol. 114, pp. 17-27, 2017.
- [5] S. H. Nie, Y. Chen, X. Ren, K. Sridharan, and T. R. Allen, "Corrosion of Alumina-Forming Austenitic Steel Fe-20Ni-14Cr-3Al-0.6Nb-0.1Ti in Supercritical Water," *Journal of Nuclear Materials*, vol. 399, no. 2-3, pp. 231-235, 2010.
- [6] I. Peter, A. Zago, M. A. Grande, and D. Ugues, "Thermo-Mechanical and Oxidation Behaviour of High Temperature Advanced Metallic Alloys," *Surface and Coatings Technology*, vol. 203, no. 13, pp. 1776-1784, 2009.
- [7] N. Parimin, and E. Hamzah, "Oxidation Kinetics of Fe-Ni-Cr Alloy at 900°C," *Materials Science Forum*, vol. 1010, pp. 58-64, 2020.
- [8] T. D. Nguyen, J. Zhang, and D. J. Young, "Effect of Mn on oxide formation by Fe-Cr and Fe-Cr-Ni alloys in dry and wet CO₂ gases at 650°C," *Corrosion Science*, vol. 112, pp. 110-127, 2016.
- [9] D. J. Young, J. Zurek, L. Singheiser, and W. J. Quadackers, "Temperature Dependence of Oxide Scale Formation on High-Cr Ferritic Steels in Ar-H₂-H₂O," *Corrosion Science*, vol. 53, no. 6, pp. 2131-2141, 2011.
- [10] D. Oquab, , N. Xu, D. Monceau, and D. J. Young, "Subsurface Microstructural Changes in a Cast Heat Resisting Alloy Caused by High Temperature Corrosion," *Corrosion Science*, vol. 52, no. 1, pp. 255-262, 2010.
- [11] D. Saber, I. S. Emam, and R. Abdel-Karim, "High temperature cyclic oxidation of Ni based superalloys at different temperatures in air," *Journal of Alloys and Compounds*, vol. 719, pp. 133-141, 2017.
- [12] J. Zurek, D. J. Young, E. Essuman, M. Hänsel, H. J. Penkalla, L. Niewolak, and W. J. Quadackers, "Growth and Adherence of Chromia Based Surface Scales on Ni-Base Alloys in High- and Low-pO₂ Gases," *Materials Science and Engineering: A*, vol. 477, no. 1-2, pp. 259-270, 2008.
- [13] N. Parimin, and E. Hamzah, "Oxide scale growth on Fe-40Ni-24Cr alloy at high temperature oxidation," *IOP Conference Series: Materials Science and Engineering*, vol. 701, no. 012022, 2019.

- [14] X. Wang, and J. A. Szpunar, "Effects of grains sizes on the oxidation behavior of Ni-based alloy 230 and N," *Journal of Alloys and Compounds*, vol. 752, pp. 40-52, 2018.
- [15] H. Z. Zheng, S. Q. Lu, and Y. Huang, "Influence of grain size on the oxidation behavior of NbCr₂ alloys at 950–1200 °C," *Corrosion Science*, vol. 51, no. 2, pp. 434–438, 2009.
- [16] X. Peng, J. Yan, Y. Zhou, and F. Wang, "Effect of grain refinement on the resistance of 304 stainless steel to breakaway oxidation in wet air," *Acta Materialia*, vol. 53, no. 19, pp. 5079–5088, 2005.
- [17] I. A. Sustaita-Torres, S. H. Rodríguez, M. P. Guerrero-Mata, M., Garza, E. Valdés, F. Deschaux-Beaume, R. Colás, "Aging of a Cast 35Cr–45Ni Heat Resistant Alloy," *Materials Chemistry and Physics*, vol. 133, pp. 1018-1023, 2012.
- [18] Y. X. Xu, J. T. Lu, X. W. Yang, J. B. Yan, Li, W. Y. (2017). Effect and role of alloyed Nb on the air oxidation behaviour of Ni-Cr-Fe alloys at 1000°C. *Corrosion Science*, Vol. 127, 10-20.
- [19] Y. X. Xu, J. T. Lu, W. Y. Li and X. W. Yang, "Oxidation behavior of Nb-rich Ni-Cr-Fe alloys: Role and effect of carbides precipitates," *Corrosion Science*, vol. 140, pp. 252-259, 2018.
- [20] L. Tan, "Corrosion Behavior of Ni-Base Alloys for Advanced High Temperature Water-Cooled Nuclear Plants," *Corrosion Science*, vol. 50, no. 11, pp. 3056–3062, 2008.
- [21] N. Parimin, E. Hamzah, A. Amrin, "Effect of solution treatment on high temperature oxidation of Fe-33Ni-19Cr and Fe-40Ni-24Cr alloys" in *Thesis PhD, Universiti Teknologi Malaysia*, pp. 272-277, 2015.